Droplet spreading driven by van der Waals force: a molecular dynamics study

2010 J. Phys.: Condens. Matter 22 325101

(http://iopscience.iop.org/0953-8984/22/32/325101)

IOP Publishing Journal of Physics: Condensed Matter

J. Phys.: Condens. Matter **22** (2010) 325101 (9pp) doi:10.1088/0953-8984/22/32/325101

Droplet spreading driven by van der Waals force: a molecular dynamics study

Congmin Wu[1], Tiezheng Qian[2] and Ping Sheng[3]

[1] Department of Mathematics, Hong Kong University of Science and Technology, Clear Water Bay, Kowloon, Hong Kong
[2] Department of Mathematics and Joint KAUST-HKUST Micro/Nanofluidics Laboratory, Hong Kong University of Science and Technology, Clear Water Bay, Kowloon, Hong Kong
[3] Department of Physics and William Mong Institute of Nano Science and Technology, Hong Kong University of Science and Technology, Clear Water Bay, Kowloon, Hong Kong

E-mail: maqian@ust.hk

Received 12 February 2010, in final form 5 May 2010
Published 7 July 2010
Online at stacks.iop.org/JPhysCM/22/325101

Abstract

The dynamics of droplet spreading is investigated by molecular dynamics simulations for two immiscible fluids of equal density and viscosity. All the molecular interactions are modeled by truncated Lennard-Jones potentials and a long-range van der Waals force is introduced to act on the wetting fluid. By gradually increasing the coupling constant in the attractive van der Waals interaction between the wetting fluid and the substrate, we observe a transition in the initial stage of spreading. There exists a critical value of the coupling constant, above which the spreading is pioneered by a precursor film. In particular, the dynamically determined critical value quantitatively agrees with that determined by the energy criterion that the spreading coefficient equals zero. The latter separates partial wetting from complete wetting. In the regime of complete wetting, the radius of the spreading droplet varies with time as $R(t) \sim \sqrt{t}$, a behavior also found in molecular dynamics simulations where the wetting dynamics is driven by the short-range Lennard-Jones interaction between liquid and solid.

(Some figures in this article are in colour only in the electronic version)

1. Introduction

The wetting phenomena of droplets on solid substrates are frequently encountered in our daily life and have found extensive industrial applications, e.g. coatings, printing, plant protection and tertiary oil recovery [1, 2]. For a complete description of wetting dynamics, it is necessary to understand the dynamic processes occurring in the immediate vicinity of the moving contact line. As first observed by Hardy [3], a microscopic thin film, called the precursor film, propagates ahead of the macroscopic spreading droplet which completely wets the substrate in the final equilibrium state. The existence of this precursor film makes the droplet spreading a complicated problem in which multiple length scales are involved. Various hydrodynamic [4–6] and molecular-kinetic [7] models and theories have been proposed and significant achievements have been made towards a more accurate and complete understanding of the wetting dynamics. While there has been rapid advances in experimental efforts, molecular dynamics (MD) simulations have been playing a very important role in our exploration of the wetting dynamics, especially at the microscopic scale.

Among the many modeling issues involved in MD simulations, the interaction between the droplet and the substrate is of central importance. When the solid substrate was modeled to be smooth by using the integrated Lennard-Jones (inverse 9–3 LJ) potential, the observed spreading rates were linear in time, i.e. $R \sim t$, where R is the radius of the wetted area at the solid surface [8–10]. For solid substrates with molecular structure, the fluid–solid interaction was modeled by an inverse 12–6 Lennard-Jones potential, and the spreading rates were found to follow the $R^2 \sim$

$\log(t)$ behavior [11]. For the spreading of liquid drops of chain molecules on a solid substrate with lattice structure, the radius of the spreading layers was found to increase with time with the square root behavior $R^2 \sim t$ [12, 13]. For the spreading of a droplet of a volatile atomic fluid on a solid substrate, the radius of the spreading layers was found to follow the square root behavior regardless of system size, lattice geometry and thermostating [14]. The $R^2 \sim t$ behavior has been observed in a few experiments [15–19]. The square root behavior was also observed in MD simulations when a long-range van der Waals-like potential was added to act on the wetting fluid [10, 12, 13]. However, only one or two values were chosen for the strength of this additional potential. In fact, MD simulations with a focus on van der Waals interactions are found to be relatively lacking, considering the role played by the long-range interactions in the hydrodynamic approaches [1].

Early MD simulations for the moving contact line [20, 21] showed that fluid slips at the solid surface in the vicinity of the contact line. Recently, through analysis of extensive MD data, the generalized Navier boundary condition was proposed to replace the no-slip boundary condition [22, 23]. A continuum description of immiscible two-phase flows at solid surfaces has been obtained by combining the generalized Navier boundary condition with the Cahn–Hilliard hydrodynamic formulation. Its numerical implementation has produced continuum solutions in quantitative agreement with MD simulation results. More recently, this continuum model has been used to investigate the development of the precursor film in droplet spreading driven by the long-range van der Waals interactions between fluid and solid [24], with the numerical results showing the dynamic wetting behavior predicted by early theoretical studies. Nevertheless, MD simulation results are not yet available for comparison with, and verification of, the results from the continuum model.

The purpose of the present paper is to carry out MD simulations to investigate the effects of a long-range, attractive van der Waals interaction between the wetting fluid and the solid. When the strength of the long-range attractive force is strong enough, a precursor film can be initiated and developed. The critical strength for the emergence of the precursor film is found to correspond to the transition from partial to complete wetting. This confirms the results from the continuum model calculations [24]. The spreading rates measured in our simulations are found to agree with experimental observations and a few other MD simulations.

This paper is organized as follows. The technical details of our MD simulations are described in section 2, followed by the simulation results presented in section 3. The critical coupling constant in the van der Waals interaction for the transition from partial to complete wetting is predicted in section 3.1. Our results for the dynamics of droplet spreading are presented in section 3.2, showing that the critical coupling constant for the emergence of the precursor film quantitatively agrees with that for the wetting transition. In section 3.3, further results are presented regarding the spreading rates. The paper is concluded in section 4 with a few remarks.

2. Molecular dynamics simulations

In our MD simulations, two immiscible fluids are confined in a rectangular box. The wetting fluid, which is going to spread later on, takes the initial shape of one-quarter of a cylinder, with the cylindrical axis parallel to the y direction. Projected onto the xz plane, the wetting fluid is initially positioned in the lower left corner of the system. This is to simulate the spreading behavior in two-dimensional (2D) space. The rest of the rectangular fluid space is filled by the other fluid, which is nonwetting. Together, the two fluids are confined in the z direction by two planar solid walls parallel to the xy plane. They are also confined in the x direction by two planar invisible walls parallel to the yz plane. Each of the two solid walls is constructed by two [001] planes of an fcc lattice, with each solid molecule attached to a lattice site by a harmonic spring. The periodic boundary condition is used in the y direction only.

The wetting and nonwetting fluids are both monatomic. The pair interaction between fluid molecules is modeled by a modified Lennard-Jones (LJ) potential $U_{\rm ff}(r) = 4\epsilon[(\sigma/r)^{12} - \delta_{\rm ff}(\sigma/r)^6]$, where r is the distance between the molecules, ϵ and σ are the energy and range parameters of the interaction, respectively, and $\delta_{\rm ff} = 1$ for like molecules and $\delta_{\rm ff} = -1$ for molecules of different species (with the immiscibility ensured by the negative $\delta_{\rm ff}$). The molecular interaction between solid wall and fluid is modeled by a modified LJ potential $U_{\rm wf}(r) = 4\epsilon_{\rm wf}[(\sigma_{\rm wf}/r)^{12} - \delta_{\rm wf}(\sigma_{\rm wf}/r)^6]$, with the energy and range parameters $\epsilon_{\rm wf} = 1.16\epsilon$ and $\sigma_{\rm wf} = 1.04\sigma$, and $\delta_{\rm wf}$ for specifying the wetting property of the fluid. We use the same wall–fluid interaction for the wetting and nonwetting fluids, mostly with $\delta_{\rm wf} = 0.8$. Both $U_{\rm ff}$ and $U_{\rm wf}$ are cut off at $r_c = 2.5\sigma$. Before the long-range van der Waals interaction between the wetting fluid and the solid wall is turned on, the fluid–fluid interface meets the solid wall with a contact angle of 90°. The two invisible walls are not constructed by molecules but simply modeled by the potential $V_{\rm ex}(x) = 4\epsilon[\frac{\pi}{45}(\frac{\sigma}{x-x_{\rm l}})^9 - \frac{\pi}{6}(\frac{\sigma}{x-x_{\rm l}})^3 + \frac{\pi}{45}(\frac{\sigma}{x_{\rm r}-x})^9 - \frac{\pi}{6}(\frac{\sigma}{x_{\rm r}-x})^3]$, which prevents the fluid molecules from escaping through the left and right boundaries. Here $x_{\rm l}$ and $x_{\rm r}$ are the x coordinates of the left and right boundaries of the simulation box. The potential $V_{\rm ex}$ is cut off at $x - x_{\rm l} = 5\sigma$ and $x_{\rm r} - x = 5\sigma$.

The droplet of the wetting fluid is forced to spread by turning on the long-range van der Waals interaction between the wetting fluid and the solid wall. This is modeled by the potential

$$U_{\rm VW}(z) = -\frac{A_{\rm p}}{3}\frac{1}{(z-z_0)^3}, \tag{1}$$

which acts on each molecule of the wetting fluid. Here z_0 is the z coordinate of the upper [001] plane of the bottom wall and z is the z coordinate of the fluid molecule. The coupling constant $A_{\rm p}$ is directly related to the Hamaker constant. That is, if the fluid has a uniform number density ρ, then the potential energy density that gives rise to the attractive van der Waals interaction between fluid and solid is of the form $-\frac{A}{6\pi}\frac{1}{(z-z_0)^3}$, where A is the Hamaker constant [1, 24], given by $A = 2\pi A_{\rm p}\rho$. Note that, because of the short-range repulsive interactions, there is always a narrow void between the fluid boundary and the solid surface, i.e. z is always larger than z_0. In the present study, $A_{\rm p}$

is the only parameter that will be varied to change the spreading behaviors. Physically, the van der Waals interaction arises from the long-range attraction ($\sim -1/r^6$) in molecular interaction potentials. In the simulations presented here, all the molecular pair interactions are truncated, and the long-range attractive van der Waals interaction is modeled by $U_{\rm VW}(z)$, introduced as an external potential acting on the wetting fluid. The $-\frac{1}{(z-z_0)^3}$ dependence results from a volume integral over the half-space that bounds the fluids from below.

The mass of a solid molecule is equal to that of a fluid molecule m. The number density of the solid wall is $\rho_w = 1.86\sigma^{-3}$. The average number density of each fluid is $\rho = 0.81\sigma^{-3}$. With each solid molecule attached to a lattice site by a harmonic spring, the Lindemann criterion is satisfied (to maintain the crystalline structure of the solid wall). The temperature is controlled at $1.4\epsilon/k_{\rm B}$ by the Langevin thermostat, where $k_{\rm B}$ is the Boltzmann constant. The equations of motion are integrated using a velocity Verlet algorithm with a time step $\Delta t = 0.001\tau$, where $\tau = \sqrt{m\sigma^2/\epsilon}$ is the time unit.

As to the size of the simulated systems, there are two major considerations. On the one hand, our purpose is to observe and measure how the spreading proceeds in space and time. The droplet of wetting fluid should be large enough to provide a continuous supply to the growing wetting film, and the substrate (i.e. the bottom wall) should be long enough to support the development of a long film. On the other hand, we need to reduce the CPU time for each time step by simulating small systems as the spreading process may be slow. In the simulations presented in this paper, the initial radius of the droplet is $R_0 = 32\sigma$. Most of the systems measure $100.7\sigma \times 7.7\sigma \times 39.9\sigma$ along the x, y and z directions. (The distance between the two planes of each solid wall is 0.65σ. Hence the distance between the inner planes (which face the confined fluids directly) of the bottom and top walls is 38.6σ.) The wetting fluid, initially confined in the lower left corner of $x^2 + (z - z_0)^2 \leqslant R_0^2$ (with $x = 0$ at the left boundary and $z_0 = 0.65\sigma$ at the upper plane of the bottom wall), is subject to the attraction towards the bottom wall through the van der Waals interaction, which is turned on immediately after the fast equilibration of fluids. There are 27 344 particles in total, including 1872 solid molecules in each wall and 4928 molecules in the spreading droplet.

A series of MD simulations have been performed with the coupling constant $A_{\rm p}$ (representing the Hamaker constant) varied in a wide range. It is observed that there exists a critical coupling constant above which a precursor film can be developed. It has been accepted for a long time that, in the regime of complete wetting characterized by a positive spreading coefficient, the spreading of a droplet is pioneered by a precursor film (see, e.g., [1], for a hydrodynamic treatment). In the present study, this rather general phenomenon has been observed in our MD simulations for two immiscible monatomic fluids on a structured solid substrate, with a long-range interaction between the wetting fluid and the substrate. We understand that there have been MD simulations which also showed some critical coupling constant for the occurrence of the precursor film, for differently modeled fluids and fluid–solid interactions [25]. To simulate long precursor films for a strong van der Waals interaction, we use systems that measure 120σ or 140σ in the x direction without changing the dimensions in the other two directions. All simulations are stopped before the tip of the precursor film approaches the right boundary in the x direction within a distance of 10σ.

To avoid the volatility of the spreading droplet, chain molecules have usually been used in MD simulations, with adjoining LJ atoms linked by the FENE potential [26, 27], by the harmonic potential [9] or by a confining potential $\sim r^6$ [12, 28, 29]. By suppressing the volatility, the polymeric liquids used in experiments can be better simulated. In our simulations, although the spreading droplet is a monatomic fluid, it is surrounded by the other immiscible fluid and hence there is no volatility at all. We would like to mention that immiscible fluids of equal density and equal viscosity have been used to simulate the contact-line motion in immiscible two-phase flows [21, 22, 30] and continuum hydrodynamic calculations have been carried out as well for these systems [23, 24, 30, 31]. We hope that the present study can serve as a starting point for future studies involving immiscible fluids of variable density and viscosity ratios.

3. Simulation results

3.1. The spreading coefficient and critical coupling constant

The dynamics of spreading is controlled by the spreading coefficient

$$S = \gamma_1 - [\gamma_2 + V_{\rm VW}(\infty)] - \gamma, \tag{2}$$

which takes into account both the short-range and long-range interactions. Here γ_1 and γ_2 are the interfacial free energies per unit area at the wall–fluid interface (with the subscripts '1' and '2' denoting the nonwetting and wetting fluids, respectively), γ is the interfacial free energy per unit area at the fluid–fluid interface and $V_{\rm VW}(\infty)$ is the potential energy per unit area accumulated in the wetting fluid due to its (attractive) van der Waals interaction with the substrate. Physically, γ_1, γ_2 and γ all arise from the short-range interactions, i.e. truncated $U_{\rm wf}(r)$ and $U_{\rm ff}(r)$. That is, these interfacial quantities can be defined whether the long-range interaction is present or not, and they are determined by the short-range interactions alone. While the long-range interaction between the wetting fluid and the substrate can be obtained by summing up the long-range tails of the $1/r^6$ interaction, the pair interactions have been cut off for computational reasons. Therefore, the long-range interaction has been modeled by adding $U_{\rm VW}(z)$ as an external potential acting on the wetting fluid. In this way, the interaction between the wetting fluid and the substrate has been compensated. The interpretation of our results is based on equation (2), in which γ_2 is supplemented by $V_{\rm VW}(\infty)$, with the former determined by the truncated pair interactions and the latter by $U_{\rm VW}(z)$. In our simulations, the two fluids have the same short-range interaction (i.e. $U_{\rm wf}$) with the solid substrate, so $\gamma_1 = \gamma_2$ and $S = -V_{\rm VW}(\infty) - \gamma$ (with $V_{\rm VW}(\infty) < 0$ due to attraction and $\gamma > 0$ due to short-range repulsion).

With $\gamma_2 + V_{\rm VW}(\infty)$ acting as the effective interfacial free energy per unit area for the wetting fluid on the solid

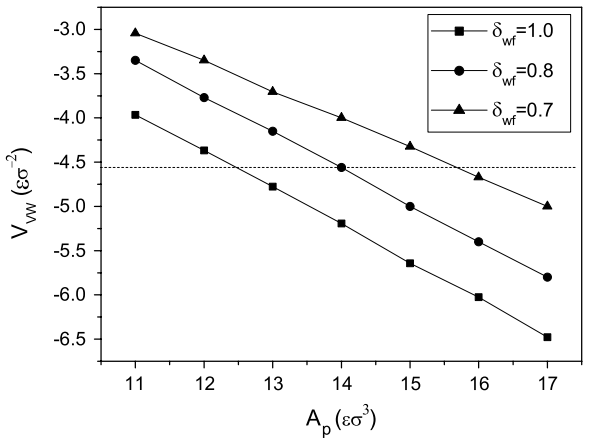

Figure 1. The van der Waals energy per unit area $V_{\rm VW}$ plotted as a function of $A_{\rm p}$ in $U_{\rm VW}$ for three different values of $\delta_{\rm wf}$ in $U_{\rm wf}$. The critical value of $A_{\rm p}$ is determined by $V_{\rm VW} = -4.55\epsilon\sigma^{-2}$ (indicated by the dotted line). A larger $\delta_{\rm wf}$ leads to a smaller critical value of $A_{\rm p}$.

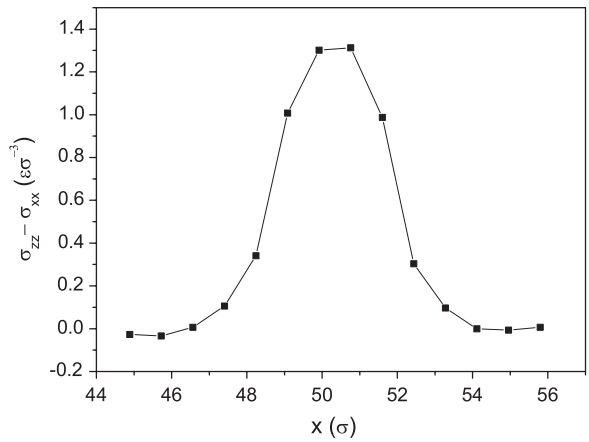

Figure 2. The stress anisotropy $\sigma_{zz} - \sigma_{xx}$ measured as a function of x in the interfacial region for a fluid–fluid interface parallel to the yz plane. The interfacial tension $\gamma = 4.55\epsilon\sigma^{-2}$ is obtained by evaluating the integral $\int_{\rm int} {\rm d}x\,(\sigma_{zz} - \sigma_{xx})$.

surface, a negative value of S leads to partial wetting while a positive value of S leads to complete wetting. That is, if $\gamma_1 > [\gamma_2 + V_{\rm VW}(\infty)] + \gamma$, then the free energy of the solid/fluid-1 (nonwetting) interface can be lowered by intercalating a film of fluid-2 (wetting), with the total free energy per unit area given by $[\gamma_2 + V_{\rm VW}(\infty)] + \gamma$. In our simulations, $V_{\rm VW}(\infty)$ and γ can both be measured and the critical value of $A_{\rm p}$ in the potential $U_{\rm VW}(z)$ can be determined by the condition $S = -V_{\rm VW}(\infty) - \gamma = 0$ for the transition from partial to complete wetting.

Given $U_{\rm VW}(z)$ as the van der Waals energy per molecule between the wetting fluid and the substrate, $V_{\rm VW}(\infty)$ is measured by calculating the sum of the van der Waals energies for all the fluid molecules. The van der Waals force acting on each fluid molecule is $-{\rm d}U_{\rm VW}/{\rm d}z = -\frac{A}{(z_i - z_0)^4}$, to be turned on immediately after the initial equilibration of fluids. The molecular density close to the substrate oscillates along the z direction and the attractive van der Waals interaction tends to increase the near-surface density. As soon as the molecular distribution is stabilized, we begin to calculate the van der Waals energies for all the fluid molecules, from which $V_{\rm VW}(\infty)$ is obtained as the time average of

$$V_{\rm VW}(\infty) = \frac{1}{s}\sum_{i\in s} U_{\rm VW}(z_i), \tag{3}$$

where s is the substrate area covered by the wetting fluid. In equation (3), $V_{\rm VW}(\infty)$ is defined as the total van der Waals energy (per unit substrate area) accumulated in the wetting fluid. This accumulation takes place in a distribution of fluid molecules in the z direction normal to the substrate. In order to let $V_{\rm VW}(\infty)$ saturate (i.e. acquire the lowest negative value), the wetting fluid has to be sufficiently thick. (The $-\frac{1}{(z-z_0)^3}$ dependence of $U_{\rm VW}(z)$ leads to a long-range tail of the energy per unit area that varies with the film thickness and tends to thicken the wetting film [1].) Figure 1 shows $V_{\rm VW}(\infty)$ as a function of $A_{\rm p}$.

To measure the fluid–fluid interfacial tension γ, a fluid–fluid interface parallel to the yz plane is stabilized (with a contact angle of 90°) and the microscopic stress anisotropy is measured as a function of x in the interfacial region (sufficiently far away from any confining wall). The interfacial tension γ is measured according to its mechanical definition [32] $\gamma = \int_{\rm int} {\rm d}x\,(\sigma_{zz}(x) - \sigma_{xx}(x))$, where $\int_{\rm int} {\rm d}x$ denotes the integration across the fluid–fluid interface along x, and σ_{zz} and σ_{xx} are the zz and xx components of the stress tensor. With the temperature fixed at $1.4\epsilon/k_{\rm B}$ and the two fluid densities fixed at $0.81/\sigma^3$, we obtain $\gamma \approx 4.55\epsilon\sigma^{-2}$ (see figure 2). So the critical value of $A_{\rm p}$ is determined by the condition $V_{\rm VW}(\infty) = -4.55\epsilon\sigma^{-2}$. We have measured $V_{\rm VW}(\infty)$ as a function of $A_{\rm p}$ for three different values of $\delta_{\rm wf}$ in the short-range wall–fluid interaction $U_{\rm wf}(r)$. The larger $\delta_{\rm wf}$ is, the more strongly are fluid molecules attracted toward the wall. With a larger near-surface density, the same amount of $V_{\rm VW}(\infty)$ can be accumulated with a smaller value of $A_{\rm p}$. Therefore, the critical value of $A_{\rm p}$ decreases with an increasing $\delta_{\rm wf}$, as shown in figure 1.

3.2. Transition from partial to complete wetting: the dynamic precursor

Before the van der Waals interaction is turned on, the wetting fluid is positioned in the lower left corner of the system and forms one-quarter of a cylinder, with a contact angle of 90°. As soon as the van der Waals interaction is turned on, a local, fast deformation of the fluid–fluid interface is initiated immediately above the real contact line. That is, the droplet undergoes a fast expansion at the bottom without changing the overall shape. Physically, the old mechanical equilibrium across the fluid–fluid interface is broken by the van der Waals interaction, which greatly increases the pressure in the wetting fluid near the lower surface. As the wetting fluid is pulled towards the solid wall, its base expands quickly and hence penetrates into the nonwetting fluid. Since the van der Waals interaction takes effect only within a narrow range (due to the (z −

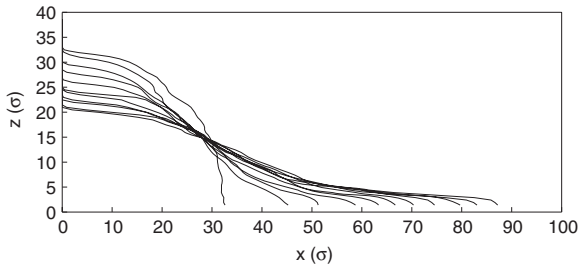

Figure 3. Time evolution of the fluid–fluid interface from $t = 0\tau$ to 4000τ, obtained for $A_p = 19\epsilon\sigma^3$ and $\delta_{wf} = 0.8$. The wetting fluid takes the initial shape of one-quarter of a cylinder (with a radius of 32σ). The spreading starts at $t = 0$ when the van der Waals interaction is turned on. Each curve is the projection of the fluid–fluid interface onto the xz plane. Each two neighboring curves are separated by a time interval of 400τ. To locate the interface, the 2D sampling region is divided into small rectangular bins, each of $\Delta x = 0.84\sigma$ by $\Delta z = 0.50\sigma$ in size. Averaging over 500 time steps in each bin yields the densities of the two fluids, from which the interface is located. Note that $500\Delta t = 0.5\tau$, very short compared to the time evolution of the interface. The system measures $100.7\sigma \times 7.7\sigma \times 39.9\sigma$ along the x, y and z directions. There are 27 344 particles in total, including 1872 solid molecules in each wall and 4928 molecules in the spreading droplet.

$z_0)^{-4}$ dependence of the attractive force), this penetration is accomplished by a thin film. In the regime of complete wetting, the total free energy can be continuously lowered if the wetting fluid acquires an ever-increasing coverage over the substrate. Therefore, the near-surface penetration proceeds through a precursor film that develops progressively ahead of the nominal contact line. (The nominal contact line refers to the edge of the macroscopic part of the droplet behind the precursor film. Were droplets of much larger size used, it would be easier to recognize the nominal contact line.) With the precursor film penetrating further into the nonwetting fluid, its tip, i.e. the real contact line, slows down due to the increased friction, presumably proportional to the film length. Meanwhile, given the limited size of the droplet, the overall shape of the wetting fluid behind the film changes noticeably because much has been transported into the developing precursor. Figure 3 shows the time evolution of the fluid–fluid interface for a spreading droplet. The results obtained for this particular case already demonstrate features commonly found in the regime of complete wetting. We want to point out that, due to the finite size of the spreading droplets used here, the nominal contact line cannot be precisely located. This may affect the accuracy in determining the critical coupling constant for the occurrence of the precursor film.

Controlled by the strength of the van der Waals interaction, the sign of the spreading coefficient S determines the shape taken by the wetting fluid in final equilibrium, which either exhibits a finite (apparent) contact angle (for partial wetting with $S < 0$) or becomes a pancake (for complete wetting with $S > 0$). (The pancake refers to a film of finite thickness due to the long-range tail of the van der Waals energy per unit area, quickly truncated towards the real contact line [1].) Physically, it is expected that the two distinct equilibria can be revealed, before they are finally reached, by different spreading behaviors. Below we present the numerical evidence for a transition in spreading dynamics controlled by the coupling constant A_p, which is varied from the regime of partial wetting to that of complete wetting.

According to figure 1, $A_p = 19\epsilon\sigma^3$ falls into the regime of complete wetting for $\delta_{wf} = 0.8$. Consequently, the precursor is formed to lead the spreading, as illustrated in figure 3. With δ_{wf} fixed at 0.8 and A_p gradually varied from $18\epsilon\sigma^3$ to $11\epsilon\sigma^3$, figure 4 shows a series of snapshots of the spreading drops, all taken at $t = 4000\tau$ (as for the last curve in figure 3). It is observed that there exists a critical value for A_p above which the spreading is pioneered by a precursor film. In particular, a larger A_p leads to a longer film, i.e. the film develops faster under a stronger attraction by the wall. Below the critical value, the spreading droplets are led by a wedge only, without a film ahead. As A_p is increased, the (negative) spreading coefficient S approaches zero and so does the apparent contact angle θ_e (with $\cos\theta_e = 1 + S/\gamma$). Though defined in equilibrium, the decreasing θ_e is already manifested by the leading wedge which becomes thinner as A_p moves closer to the critical value. According to figure 4, the critical value of A_p, by which the two distinct spreading behaviors are separated, is somewhere between $14\epsilon\sigma^3$ and $15\epsilon\sigma^3$, in agreement with that determined by the energy criterion in figure 1.

Figure 5 shows the time evolution of the fluid–fluid interface for three different values of A_p, with δ_{wf} fixed at 1.0. No noticeable difference is seen as A_p changes from $12\epsilon\sigma^3$ to $13\epsilon\sigma^3$: the spreading is led by a wedge only. The precursor film shows up, however, as A_p reaches $14\epsilon\sigma^3$. This indicates that the critical value of A_p is between $13\epsilon\sigma^3$ and $14\epsilon\sigma^3$, smaller than that for $\delta_{wf} = 0.8$, as indicated in figure 4. While this trend agrees with that predicted by the energy criterion in figure 1, the agreement is only semi-quantitative. (Figure 1 predicts the critical value to be between $12\epsilon\sigma^3$ and $13\epsilon\sigma^3$ for $\delta_{wf} = 1.0$.) The small discrepancy may be attributed to the small thickness of the film, and the change of the fluid–fluid interfacial tension γ by the proximity of the wall.

While a transition in spreading characteristics can be visually confirmed from figures 4 and 5, a more quantitative measure is needed to better locate the transition point. Physically, the precursor film extends from the nominal contact line to the real contact line. However, due to the limited size of droplets in MD simulations, the nominal contact line cannot be unambiguously located. From those snapshots taken for different spreading droplets, we find that, though the nominal contact line cannot be pinpointed, the precursor film always extends out of the wedge with a thickness of about three molecular layers. Accordingly, the length of the precursor film is approximately defined as the x distance from the real contact line to the position where the film thickness is 3σ. Figure 6 shows the film length as a function of A_p for different times. For $A_p \leqslant 15\epsilon\sigma^3$, this length never exceeds 5σ and does not increase in time. For $A_p > 15\epsilon\sigma^3$, however, the film length shows a continuous increase with time, and this increase is faster for larger A_p. From these results, the transition is located near $A_p = 15\epsilon\sigma^3$. In spite of the strong fluctuation, this agrees with the observation in figure 4 and also the critical value determined in figure 1. Finally, we want to describe

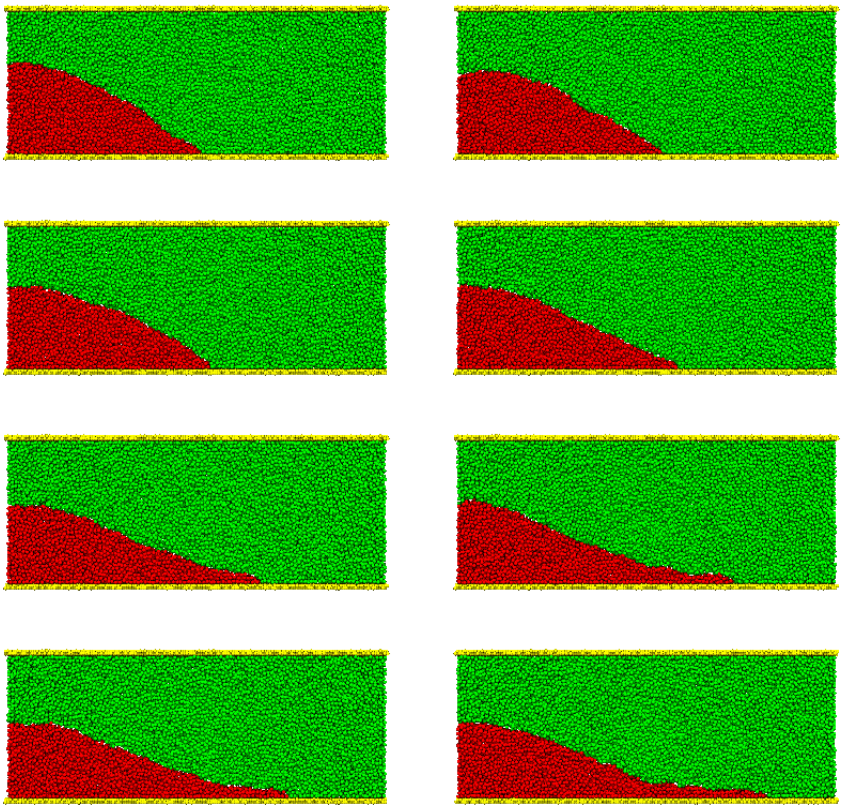

Figure 4. Snapshots of the spreading droplets at $t = 4000\tau$, obtained for $A_p = 11\epsilon\sigma^3$, $12\epsilon\sigma^3$, ..., and $18\epsilon\sigma^3$, with $\delta_{wf} = 0.8$. Here A_p increases from left to right, then from top to bottom. All the molecular positions are projected on the xz plane.

some features of the fluctuation. Close to the critical value of A_p, the film shows a strong fluctuation in its thickness, i.e. molecules supplied by the wedge are frequently used to thicken the film rather than to lengthen the film. (In the continuum description, the equilibrium thickness of the pancake scales with the spreading coefficient S as $\sqrt{\gamma/S}$ [1]. Therefore, a strong fluctuation in thickness is expected for $S \to 0^+$.) A recent study has shown that droplet spreading can be enhanced by thermal fluctuations [33]. For A_p well above the critical value, the first layer of wetting fluid may be pinned by the substrate from time to time due to the strong attraction.

3.3. The rate of spreading

How fast a droplet spreads on a substrate has been studied for decades. Factors affecting the rate of spreading include the microstructure of the droplet, the interaction between the droplet and the substrate, the nature of the substrate, etc. There have been many MD simulations performed to clarify the various effects of these factors. Among these MD simulations, however, the van der Waals interaction between the wetting fluid and the substrate has seldom been explicitly taken into account in the form of a quasi-long-range interaction with power-law dependence on normal distance (z). Physically, the long-range part of the interaction, which can be included in the so-called disjoining pressure, has been proved to be important to the static and dynamic wetting phenomena [1, 34]. In particular, it has been shown experimentally that the Hamaker constant can be continuously varied on chemically modified silica surfaces [35]. Therefore, it is necessary to carry out MD simulations to investigate the effects of the van der Waals interaction on spreading droplets.

Figure 7 shows how the base radius of the spreading droplet grows as a function of time. The diffusive spreading behavior $R(t) \sim \sqrt{t}$ has been observed in many experiments [15–19] and MD simulations [10, 12, 14, 26, 28, 29, 36, 37]. In fact, this spreading behavior dates back to the Lucas–Washburn equation [38, 39]. There have also been different spreading behaviors reported from MD simulations. Bekink *et al* [14] pointed out that the penetration of fluid atoms in the solid lattice leads to a subdiffusive regime for layer spreading, with $R(t) \sim \sqrt{\log_{10} t}$ [11]. Linear spreading behavior was reported for the spreading of a nonvolatile liquid drop on a homogeneous solid substrate that is continuous without atomic structure [8, 10]. The results in figure 7 show $R(t) \sim \sqrt{t}$ for A_p above the critical value $15\epsilon\sigma^3$ but below $\sim 20\epsilon\sigma^3$. Further increasing A_p leads to a time dependence of R faster than $\sqrt{t}$. The $R(t) \sim \sqrt{t}$ behavior observed in our simulation can be attributed to (i) the spreading drop, surrounded by the other immiscible fluid, is nonvolatile, (ii) there is no penetration into the substrate and (iii) the substrate has atomic lattice structure, by which a viscous coupling between the fluid and

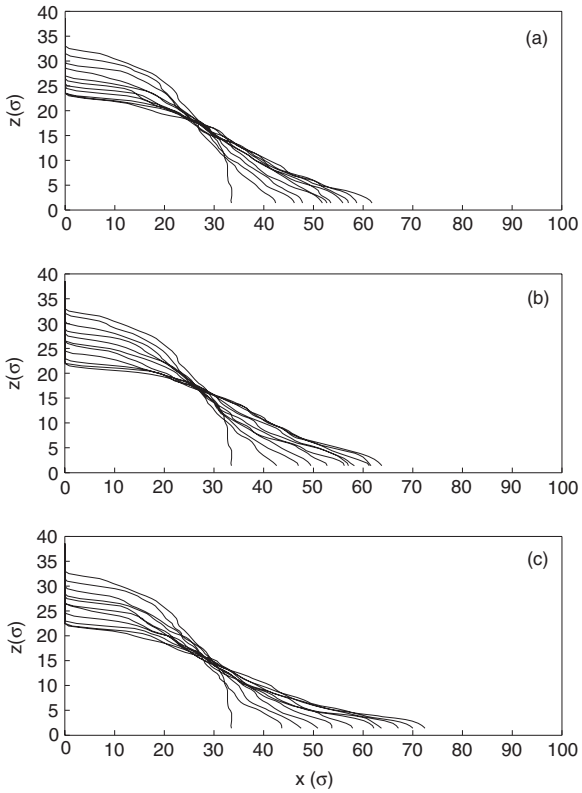

Figure 5. Time evolution of the fluid–fluid interface from $t = 0\tau$ to 4000τ, obtained for $A_p = 12\epsilon\sigma^3$ (a), $13\epsilon\sigma^3$ (b) and $14\epsilon\sigma^3$ (c), with $\delta_{wf} = 1.0$. Each two neighboring curves are separated by a time interval of 400τ.

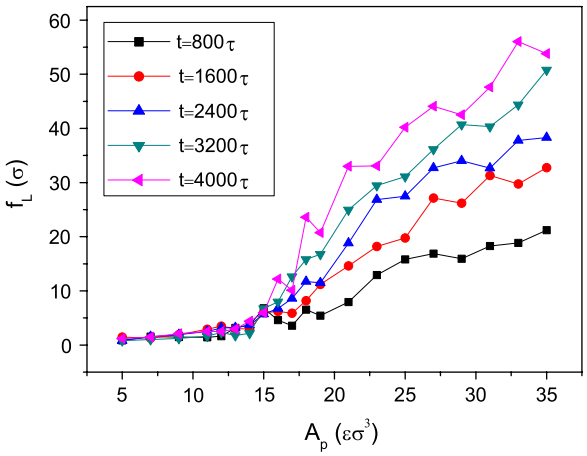

Figure 6. Precursor film length plotted as a function of A_p for different times, with δ_{wf} fixed at 0.8. The film length is measured from the real contact line to the position where the film thickness is 3σ.

the solid is induced. These are key features of the precursor film in many experiments and simulations [40]. The deviation from the $R(t) \sim \sqrt{t}$ behavior for extremely large A_p (way above the critical value for complete wetting) is an interesting observation but may not be of practical value. This deviation might arise from the finite size of the spreading droplets which are quickly depleted by the fast growing film.

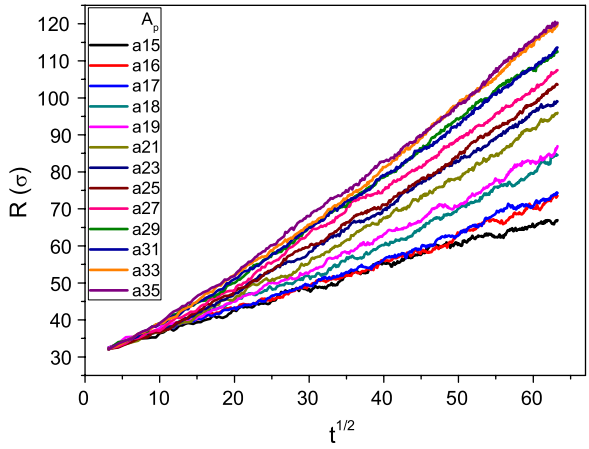

Figure 7. The base radius of the spreading droplet R, measured from the position of the real contact line, is plotted as a function of the square root of time t, with δ_{wf} fixed at 0.8 and A_p varied from $15\epsilon\sigma^3$ to $35\epsilon\sigma^3$.

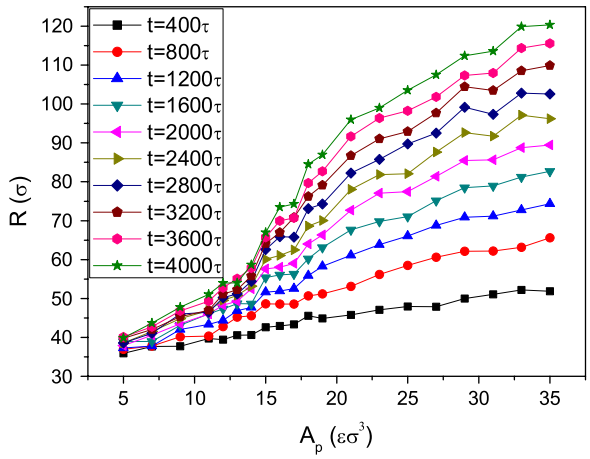

Figure 8. The base radius R plotted as a function of A_p for different times, with δ_{wf} fixed at 0.8.

It has been pointed out that strong fluid–solid interactions increase both the driving force and the resistance in wetting dynamics, while weak interactions decrease both the driving force and the resistance [41]. The two effects usually do not cancel out because of their complicated dependences on the interaction strength. Figure 8 shows the dependence of the base radius R on the coupling constant A_p. It is seen that, above the critical value $15\epsilon\sigma^3$, R increases with the increasing A_p due to the increasing driving force, but with a decreasing slope due to the increasing resistance. Physically, the development of the precursor film is driven by the positive spreading coefficient $S = -V_{VW}(\infty) - \gamma$, which increases linearly with $A_p - 15\epsilon\sigma^3$ (with $15\epsilon\sigma^3$ being the critical value for the transition from partial to complete wetting). It has been shown that, in approaching the real contact line, the film is truncated at a thickness $\propto\sqrt{\gamma/S}$ [1]. Therefore, an increase of S tends to make the film thinner, leading to an increase in viscous dissipation (due to a tighter confinement) and an increase in fluid–solid friction as well (due to a closer proximity of the fluid to the substrate). Consequently, the

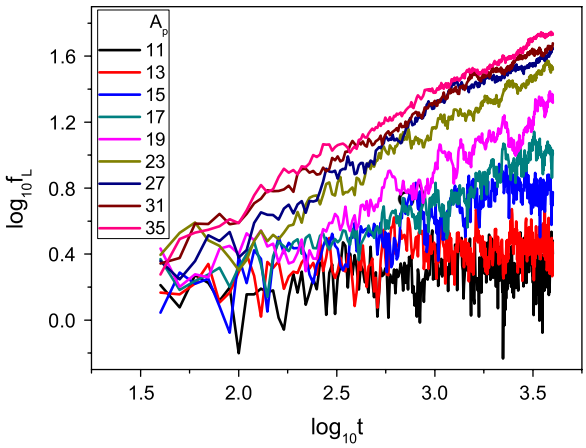

Figure 9. The film length f_L plotted as a function of time for different values of A_p, with δ_{wf} fixed at 0.8.

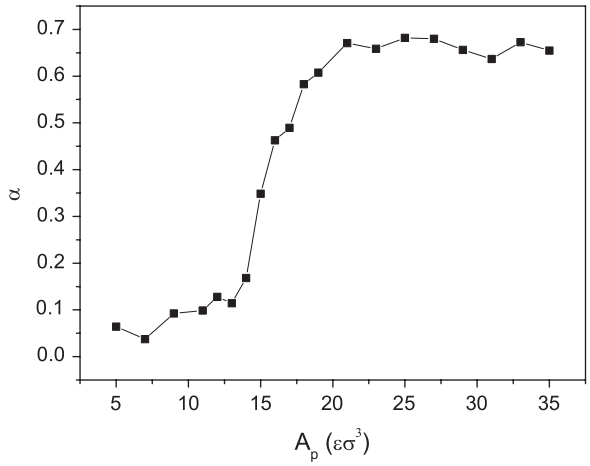

Figure 10. With f_L in figure 9 fitted by $\log_{10} f_L = \alpha \log_{10} t + \beta$, the exponent α is plotted as a function of A_p.

increase of R with A_p is slowed down when A_p becomes very large. It is also interesting to note that, across the critical value $15\epsilon\sigma^3$, the curves for R versus A_p show the steepest variation, an indicator of the formation of the precursor film. This feature becomes more transparent in the continuum calculation based on a continuum model that takes into account the contact-line slip and the van der Waals interaction explicitly (see figure 4 in [24]). While the spreading dynamics shown in our MD simulation is consistent with that in the corresponding continuum calculation, we want to point out that the time duration explored in our MD simulation is, in fact, quite short, corresponding to the initial stage of the continuum calculation. Nevertheless, we are still able to observe that, for at a given time, the curve becomes the steepest at $A_p = 15\epsilon\sigma^3$, and this feature becomes more apparent at later times. The transition so indicated agrees with the result in section 3.2.

In figure 6, the film length f_L was plotted as a function of A_p to exhibit the transition. Figure 9 shows f_L as a function of time t in a log–log plot. It is seen that below $A_p = 15\epsilon\sigma^3$, there is no visible increase of f_L with t as seen from the very noisy data. In this regime, f_L defined in figure 6 is actually contributed by the tiny front of the wedge that makes a finite contact angle. Above $A_p = 15\epsilon\sigma^3$, the film develops according to the power law $\log_{10} f_L = \alpha \log_{10} t + \beta$. Figure 10 shows the variation of the exponent α with A_p, with α simply fluctuating a bit above zero for $A_p \leqslant 15\epsilon\sigma^3$. The transition from partial to complete wetting is now clearly demonstrated by the steep jump of α around $A_p = 15\epsilon\sigma^3$. It is ready to be seen that, for $A_p \geqslant 20\epsilon\sigma^3$, α reaches and stays around 0.65. This is qualitatively consistent with what we have observed in figure 7: the base radius R follows $R(t) \sim \sqrt{t}$ for $15\epsilon\sigma^3 < A_p < 20\epsilon\sigma^3$ and shows a time dependence faster than $\sqrt{t}$ for $A_p > 20\epsilon\sigma^3$. We note that f_L (in figures 6, 9 and 10) has been defined as the x distance from the real contact line to the position where the film thickness is 3σ (see section 3.2). If we use 5σ instead, the saturation value of α becomes 0.6 approximately, indicating a film development faster than $\sqrt{t}$. More simulation results are yet to be collected to clarify the additional effect of the long-range van der Waals force on the rate of spreading.

4. Concluding remarks

MD simulations have been carried out to investigate the dynamics of droplet spreading driven by a long-range, attractive van der Waals interaction between the wetting fluid and the substrate. It has been demonstrated that, if the coupling constant in the van der Waals force is above a critical value, a precursor film can be initiated and developed. Furthermore, this dynamically determined critical coupling constant is found to quantitatively agree with the equilibrium transition point at which the spreading coefficient is zero. Therefore, the results first obtained from the continuum model calculations [24] have been confirmed. The spreading rates measured in our simulations also agree with experimental observations and a few other MD simulations.

We would like to point out that, to save the time of computation, very strong van der Waals forces have been used in simulating the initiation and development of precursor films. That makes the spreading coefficient S not very small compared to the interfacial tension γ. As a consequence, the precursor films are of molecular-scale thickness ($\sim\sqrt{\gamma/S}$) and also develop quickly. It has been shown that Tanner's law for spreading can be recovered even if the truncated van der Waals effects and the resulting precursor film are limited to distances of the order of three atomic diameters from the substrate [42]. If we want to investigate the dynamic details within the precursor film (e.g. slip, for comparison with continuum predictions), a much smaller S is required to generate a thicker film with slower dynamics, for which the MD simulations would be more costly. Work in this direction is currently underway.

Acknowledgments

This publication was based on work supported in part by award no. SA-C0040/UK-C0016, made by the King Abdullah University of Science and Technology (KAUST), Hong Kong RGC grant no. 602007 and the Croucher Foundation grant

Z0138. We would like to thank Yana Di and Xiao-Ping Wang for helpful discussions.

References

[1] de Gennes P G 1985 Wetting: static and dynamics *Rev. Mod. Phys.* **57** 827–63

[2] Bonn D, Eggers J, Indekeu J, Meunier J and Rolley E 2009 Wetting and spreading *Rev. Mod. Phys.* **81** 739–805

[3] Hardy W B 1919 The spreading of fluids on glass *Phil. Mag.* **38** 49–55

[4] Huh C and Scriven L E 1971 Hydrodynamic model of steady movement of a solid/liquid/fluid contact line *J. Colloid Interface Sci.* **35** 85–101

[5] Cox R G 1986 The dynamics of the spreading of liquids on a solid surface. Part 1. Viscous flow *J. Fluid Mech.* **168** 169–94

[6] Voinov O V 1976 Hydrodynamics of wetting *Fluid Dyn.* **11** 714–21

[7] Blake T D and Haynes J M 1969 Kinetics of liquid/liquid displacement *J. Colloid Interface Sci.* **30** 421–3

[8] Nieminen J A, Abraham D B, Karttunen M and Kaski K 1992 Molecular dynamics of a microscopic droplet on solid surface *Phys. Rev. Lett.* **69** 124–7

[9] Nieminen J A and Ala-Nissila T 1994 Spreading dynamics of polymer microdroplets: a molecular-dynamics study *Phys. Rev.* E **49** 4228–36

[10] van Remoortere P, Mertz J E, Scriven L E and Davis H T 1999 Wetting behavior of a Lennard-Jones system *J. Chem. Phys.* **110** 2621–8

[11] Yang J X, Koplik J and Banavar J R 1991 Molecular dynamics of drop spreading on a solid surface *Phys. Rev. Lett.* **67** 3539–42

[12] De Coninck J, D'Ortona U, Koplik J and Banavar J R 1995 Terraced spreading of chain molecules via molecular dynamics *Phys. Rev. Lett.* **74** 928–31

[13] D'Ortona U, Coninck J D, Koplik J and Banavar J R 1996 Terraced spreading mechanisms for chain molecules *Phys. Rev.* E **53** 562–9

[14] Bekink S, Karaborni S, Verbist G and Esselink K 1996 Simulating the spreading of a drop in the terraced wetting regime *Phys. Rev. Lett.* **76** 3766–9

[15] Heslot F, Fraysse N and Cazabat A M 1989 Molecular layering in the spreading of wetting liquid drops *Nature* **338** 640–2

[16] Heslot F, Cazabat A M and Levinson P 1989 Dynamics of wetting of tiny drops: ellipsometric study of the late stages of spreading *Phys. Rev. Lett.* **62** 1286–9

[17] Heslot F, Cazabat A M, Levinson P and Fraysse N 1990 Experiments on wetting on the scale of nanometers: influence of the surface energy *Phys. Rev. Lett.* **65** 599–602

[18] Moon J, Lowekamp J, Wynblatt P, Garoff S and Suter R M 2001 Effects of concentration dependent diffusivity on the growth of precursing films of Pb on Cu(111) *Surf. Sci.* **488** 73–82

[19] Biance A L, Clanet C and Quere D 2004 First steps in the spreading of a liquid droplet *Phys. Rev.* E **69** 016301

[20] Koplik J, Banavar J R and Willemsen J F 1988 Molecular dynamics of Poiseuille flow and moving contact lines *Phys. Rev. Lett.* **60** 1282–5

[21] Thompson P A and Robbins M O 1989 Simulations of contact-line motion: slip and the dynamics contact angle *Phys. Rev. Lett.* **63** 766–9

[22] Qian T, Wang X-P and Sheng P 2003 Molecular scale contact line hydrodynamics of immiscible flows *Phys. Rev.* E **68** 016306

[23] Qian T Z, Wang X P and Sheng P 2006 A variational approach to moving contact line hydrodynamics *J. Fluid Mech.* **564** 333–60

[24] Di Y N and Wang X P 2009 Precursor simulations in spreading using a multi-mesh adaptive finite element method *J. Comput. Phys.* **228** 1380–90

[25] Voue M, Valignat M P, Oshanin G, Cazabat A M and De Coninck J 1998 Dynamics of spreading of liquid microdroplets on substrates of increasing surface energies *Langmuir* **14** 5951–8

[26] Heine D R, Grest G S and Webb E B III 2003 Spreading dynamics of polymer nanodropets *Phys. Rev.* E **68** 061603

[27] Heine D R, Grest G S and Webb E B III 2004 Spreading dynamics of polymer nanodroplets in cylindrical geometries *Phys. Rev.* E **70** 011606

[28] Coninck J D and Blake T D 2008 Wetting and molecular dynamics simulations of simple liquids *Annu. Rev. Mater. Res.* **38** 1–22

[29] Wu X H, Phan-Thien N, Fan X J and Ng T Y 2003 A molecular dynamics study of drop spreading on a solid surface *Phys. Fluid* **15** 1357–62

[30] Ren W Q and E W 2007 Boundary conditions for the moving contact line problem *Phys. Fluids* **19** 022101

[31] Qian T Z, Wu C M, Lei S L, Wang X P and Sheng P 2009 Modeling and simulations for molecular scale hydrodynamics of moving contact line in immiscible two-phase flows *J. Phys.: Condens. Matter* **21** 464119

[32] Kirkwood J G and Buff F P 1949 The statistical mechanical theory of surface tension *J. Chem. Phys.* **17** 338–43

[33] Willis A M and Freund J B 2009 Enhanced droplet spreading due to thermal fluctuations *J. Phys.: Condens. Matter* **21** 464128

[34] Bonn D and Ross D 2001 Wetting transitions *Rep. Prog. Phys.* **64** 1085–163

[35] Silberzan P and Leger L 1995 Evidence for a new spreading regime between partial and total wetting *Phys. Rev. Lett.* **66** 185–8

[36] Webb E B III, Grest G S and Heine D R 2003 Precursor film controlled wetting of Pb and Cu *Phys. Rev. Lett.* **91** 236102

[37] Dimitrov D I, Milchev A and Binder K 2007 Capillary rise in nanopores: molecular dynamics evidence for the Lucas-Washburn equation *Phys. Rev. Lett.* **99** 054501

[38] Lucas R 1918 Rate of capillary ascension of liquids *Kolloid Z.* **23** 15–22

[39] Washburn E W 1921 The dynamics of capillary flow *Phys. Rev.* **17** 273–83

[40] De Coninck J, de Ruijter M J and Voue M 2001 Dynamics of wetting *Curr. Opin. Colloid Interface Sci.* **6** 49–53

[41] Blake T D and De Coninck J 2002 The influence of solid–liquid interactions on dynamic wetting *Adv. Colloid Interface Sci.* **96** 21–36

[42] He G and Hadjiconstantinou N G 2003 A molecular view of Tanner's law: molecular dynamics simulations of droplet spreading *J. Fluid Mech.* **497** 123–32